Ultramicroscopy 203 (2019) 60–67

Contents lists available at ScienceDirect

Ultramicroscopy

journal homepage: www.elsevier.com/locate/ultramic

# Progress in ultrahigh energy resolution EELS

O.L. Krivanek[a,b,*], N. Dellby[a], J.A. Hachtel[c], J.-C. Idrobo[c], M.T. Hotz[a], B. Plotkin-Swing[a], N.J. Bacon[a], A.L. Bleloch[a], G.J. Corbin[a], M.V. Hoffman[a], C.E. Meyer[a], T.C. Lovejoy[a]

[a] Nion R&D, 11511 NE 118th St, Kirkland, WA 98034, USA
[b] Department of Physics, Arizona State University, Tempe, AZ 85287, USA
[c] Center for Nanophase Materials Sciences, Oak Ridge National Laboratory, Oak Ridge, TN 37831, USA

A B S T R A C T

Electron energy loss spectroscopy (EELS) in the electron microscope has progressed remarkably in the last five years. Advances in monochromator and spectrometer design have improved the energy resolution attainable in a scanning transmission electron microscope (STEM) to 4.2 meV, and new applications of ultrahigh energy resolution EELS have not lagged behind. They include vibrational spectroscopy in the electron microscope, a field that did not exist 5 years ago but has now grown very substantially. Notable examples include vibrational mapping with about 1 nm spatial resolution, analyzing the momentum dependence of vibrational states in very small volumes, determining the local temperature of the sample from the ratio of energy gains to energy losses, detecting hydrogen and analyzing its bonding, probing radiation-sensitive materials with minimized damage by aloof spectroscopy and leap-frog scanning, and identifying biological molecules with different isotopic substitutions. We review the instrumentation advances, provide a summary of key applications, and chart likely future directions.

## 1. Introduction

Professors Christian Colliex, Archie Howie and Hannes Lichte have had a huge impact on electron microscopy, as pioneering researchers, educators and leaders. Telling examples of their influence are provided by the research histories of the authors of this paper: olk and alb received a thorough grounding in scientific research while studying for their Ph.D.s with Archie Howie, olk and nd benefitted, during the development of their first aberration corrector, from the wonderful hospitality of the Brown and Howie Microstructure Physics group in the Cavendish Laboratory, olk learned about EELS and STEM while working in Christian Colliex's Orsay STEM group for almost a year (distributed over several visits), and all the authors have been greatly inspired by Hannes Lichte's scientific work and public service. It is very appropriate and a great pleasure to dedicate this paper to them.

Electron microscopy and EELS have a rich history that spans many decades. A theme running through the various stages of their progress is that when a fundamentally new capability is developed, applications emerge that were impossible to predict before the capability existed. This is of course nothing new: the discoveries of Galileo with the telescope [1] and van Leeuwenhoek with the microscope [2] were precisely of this kind. It is nevertheless very gratifying that the approach of developing new instruments first and identifying what they are best for second is a fruitful one even in the 21st century, despite today's vast knowledge base. Without this element of surprise, developing new instruments would not be nearly as exciting.

## 2. Improvements in EELS energy resolution

EELS in an electron probe-forming instrument was introduced in 1943–4 by Hillier and Baker [3,4], who obtained spectra from small sample areas using an analyzer of 20–75 keV primary energy, with an energy resolution of one part in 5000 (i.e., 8 eV for a 40 keV primary beam) and spatial resolution of about 200 nm. They were able to identify carbon, oxygen and silicon by their K-edges, but further progress was largely prevented by hydrocarbon contamination in their vacuum system. The technique was reprised in the 1960 s and 1970 s, and minimized contamination problems by using cleaner vacuum techniques and/or analyzing wider sample areas. Cold field emission guns with reduced energy spread plus improved stabilities allowed the energy resolution to improve to ~0.3 eV [5–7]. Studies of EELS fine structures thus became possible, both in the low loss region [8] and at core loss edges [9], and became easier with the introduction of efficient parallel detection systems (e.g. [10]). Further progress in energy resolution was limited by the energy width of available electron sources to about 0.3 eV.

Electron-optical monochromators allow the energy resolution to be improved beyond the energy width of the source. Their development dates back to an energy analyzer built by Wien [11], whose principle was used by Boersch and Geiger for both the monochromator and the analyzer in a broad-beam EELS system that eventually reached 3 meV energy resolution at 25–30 keV [12,13]. Subsequent monochromator developments proceeded on two parallel paths: monochromators for

* Corresponding author at: Nion R&D, 11511 NE 118th St, Kirkland, WA 98034, USA.
*E-mail address:* krivanek@nion.com (O.L. Krivanek).

https://doi.org/10.1016/j.ultramic.2018.12.006
Received 1 November 2018; Received in revised form 8 December 2018; Accepted 9 December 2018
Available online 11 December 2018
0304-3991/ 

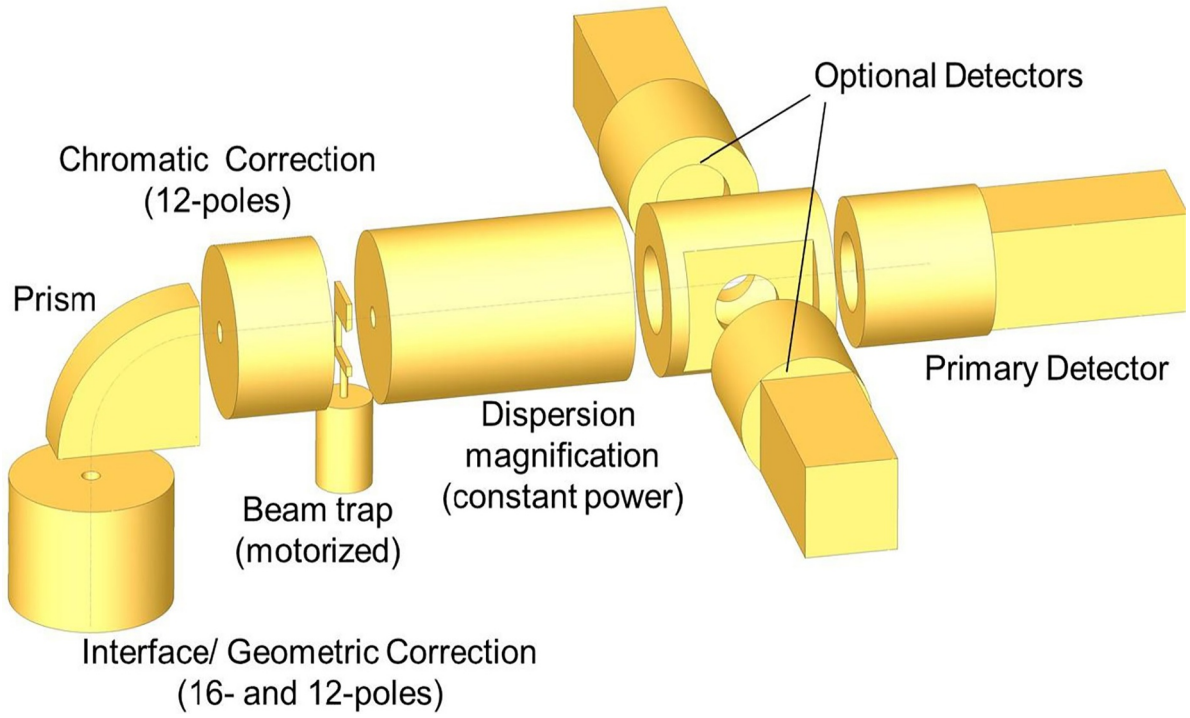


**Fig. 1.** Schematic of the Nion Iris spectrometer designed for 30–200 keV. The spectrometer is interfaced to the pre-spectrometer detector module located at the top of the Nion STEM. Important details such as triple layer magnetic shielding and sturdy mechanical supports have been omitted for clarity.

broad-beam systems, which reached meV-level energy resolution when used for reflection EELS with primary beam energies < 10 eV [14], and monochromators for transmission electron microscopes aiming at good spatial resolution, either by forming narrow beams with pre-sample optics, or by forming images with post-sample optics. The progress in monochromators for transmission electron microscopes has been reviewed by Tsuno [15], Kimoto [16] and Hawkes and Krivanek [17].

In 2010, energy resolution of 43 meV was reached at 200 keV primary energy in a monochromated microscope that allowed regular imaging and analysis [18]. This was a substantial achievement: an energy resolution of 2 parts in $10^7$ in a system which used no stabilizing schemes to tie the high voltage to the energy selected by its imaging filter/spectrometer, and therefore needed to stabilize its high voltage and spectrometer prism power supplies to even higher levels. Better energy resolution was however obtainable by making the energy resolution insensitive to variations in the microscope high voltage and in the power supplies for its energy-dispersing elements. The standard approach to achieving this was to put the monochromator and the spectrometer on a shared high voltage, which led to an energy resolution of 12 meV at 60 kV with a small beam current in a substantially modified electron microscope [19], and 25 meV with a beam current sufficient for spectroscopic investigations, with probe sizes of 30–110 nm Ø.

Putting the monochromator and the spectrometer at the high voltage meant that the electron beam was energy-dispersed at beam energies as low as a few tens of eV. This guaranteed high energy dispersion and lessened the sensitivity to stray magnetic fields compared to monochromators operating on full beam energy, but it implied two disadvantages. One, low energy electrons are more sensitive to stochastic Coulomb broadening known as the Boersch effect [20] than high energy electrons, and two, the deceleration needed just in front of the analyzer was not practical, particularly for electron energies > 100 keV.

A way around these difficulties was proposed in 1991 (see [21], Fig. 9): purely magnetic monochromator and spectrometer placed at ground potential, with their magnetic prisms all connected in series and using the same power supply. This arrangement made the energy selected by the monochromator independent of the high tension (HT) of the microscope, and also guaranteed that variations in the prism current would not degrade the energy resolution. A potential weakness was that with no connection between the energy selected by the monochromator's prisms and the HT, the energy-dispersed beam projected onto the monochromator's energy-selecting slit would have been free to move and even wander completely off the slit. The proposed scheme resolved this by monitoring the beam current falling on the two slit halves, and feeding the difference signal to the HT in a fast feedback loop that kept the beam centred on the slit. Two other weaknesses were however not addressed in the proposal: (1) the monochromator did not undisperse the electron beam at its exit, which would have led to a loss of beam brightness, and (2) the spectrum incident on the monochromator's energy-selecting slit was produced by the prisms of an omega filter, with no provision for extra magnification, and this would have limited the attainable energy resolution.

These difficulties were corrected in an improved design that was published 18 years later [22]. Its monochromator used a dispersing-undispersing alpha filter arrangement, and it incorporated quadrupoles to magnify the spectrum at the energy-selecting slit, typically by about 100x relative to the spectrum produced by the monochromator's primary prism. This proposal led to a practical implementation [23,24], which achieved 12 meV energy resolution in a 2 ms spectrum at 60 keV primary energy in 2012. The energy resolution then became limited by the EEL spectrometer [25], which used independent power supplies for each pole, an arrangement that resulted in dipole-type instabilities that randomly wobbled the electron beam on the EELS detector.

Developing an ultra-high energy resolution spectrometer which would be diffraction-limited [26] rather than instability-limited thus became an important priority [27] for Nion. Our new spectrometer [28], called Iris, uses the same multipole arrangement as the one employed by the Nion aberration correctors and monochromator: the coils of each multipole are all connected in series, eliminating the deleterious dipole moments. It corrects spectrum aberrations up to 5th order, by the use of 16-poles that are energized to produce multipole moments up to

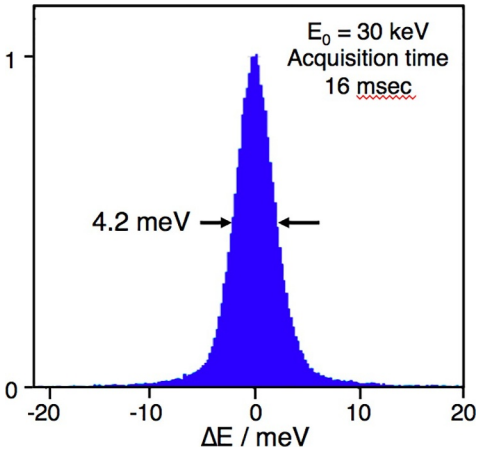


**Fig. 2.** Zero loss peak (ZLP) recorded in the vacuum outside a sample with the Nion Iris. 30 keV primary energy, 20 mrad illumination and collection half-angles, 0.2 meV/channel, 16 msec acquisition time. The intensity of the ZLP tail at 20 meV energy loss is ~0.001 of the ZLP maximum.

rotatable 12-poles, and has triple μ-metal shielding, mechanical construction that minimizes vibrations, and 9 quadrupole stages after the prism that can magnify the energy dispersion to as high as 0.1 meV per channel (at 60 keV primary energy). The prism is a gradient one that focuses the beam in both x and y directions, there is a movable beam trap that can be inserted at different heights in the beam path, and a flexible detector chamber that allows up to 3 different types of detectors to be mounted simultaneously. The spectrometer design is shown schematically in Fig. 1.

Fig. 2 shows a monochromated zero loss peak (ZLP) obtained by Iris at 30 keV primary energy, in 16 msec - an acquisition time that integrates over 98% of a cycle of the North American AC mains and thus shows the effect of instabilities due to mains interference. The measured energy resolution (full width at half maximum (FWHM)) of the ZLP is 4.2 meV, roughly equalling the energy resolution performance of the Boersch–Geiger broad-beam system [13]. Also very importantly, the intensity at 20 meV energy loss, measured with no sample, is < 0.001 of the ZLP maximum intensity, precisely as needed for exploring low energy features. The monochromator is compatible with forming ~1 Å diameter electron probes at primary energies of 30 keV and higher [29], and it is designed for ultra-high vacuum (UHV), with no single O-ring vacuum seals. At higher primary energies, the measured energy resolution grows worse approximately as the square root of the primary energy $\sqrt{E_o}$, achieving 5.7 meV at $E_o$ = 60 keV, 8.0 meV at 100 keV, and 14.7 meV at 200 keV. The absolute energy resolution can therefore be better than 1 part in $10^7$–a remarkable improvement on Hillier and Baker's 1 part in 5000.

## 3. Applications of ultra-high energy-resolution EELS

The applications that have been enabled by the progress in the energy resolution can be divided into two broad classes: readily foreseeable, and rather surprising.

Improving experiments that could previously be carried out at a worse energy resolution is rather straightforward, and new experiments inspired by equivalents such as broad-beam EELS or infrared spectroscopy are not surprising either. This type of progress has included more precise determination of band gaps in materials [30,31], and the opening up of vibrational spectroscopy in the electron microscope [32,33]. More unexpected findings were largely due to the spatial variation of very low-energy EELS carried out with a nm-sized electron probe instead of a broad beam. There was of course pioneering work in this field, with early observations of the spatial variation including aloof geometry of low loss EELS carried out by Batson [34,35], theoretical underpinning provided by Howie and co-workers [36,37], and further contributions from Christian Colliex's group plus collaborators [38]. However, the richness of the new types of information that became available took many of us by surprise.

Limited vibrational spectroscopy becomes possible in an electron microscope at around 30 meV energy resolution, and the information becomes progressively richer as the energy resolution is improved. Combined with excellent spatial and angular resolution, vibrational spectroscopy in the electron microscope is now ripening into a major new body of experimental and theoretical work.

Starting with the basic findings, Dwyer et al. demonstrated that there are both localized and delocalized vibrational interactions, and that they are separated in angular space [39]. The delocalized interactions can be selected by using a “bright field“ EELS collection geometry, in which the bright field cone enters the spectrometer and small scattering angles and large delocalization predominate, whereas “dark field” EELS, in which the bright field cone is excluded and the admitted scattering events correspond to larger scattering angles, gives much better spatial localization [39]. The cross-section for the delocalized scattering is usually larger and when the two types of signal are mixed, the delocalized interaction typically dominates. But there are counter-examples such as bulk phonons in MgO cubes, which can be mapped with < 2 nm spatial resolution with no angular selection [40,41]. The spatially extended scattering is mediated by dipole interaction and is often due to phonon polaritons [42]. It can be excited by electrons passing tens and even hundreds of nm away from the excited object, and the corresponding experimental technique is therefore named “aloof EELS”. Aloof EELS results in greatly reduced radiation damage, a theme that is reprised in the discussion section of this article.

Exploring the momentum dependence of phonons and identifying different phonon modes including acoustic ones [43] was a logical next step. The resultant energy-momentum (ω-q) information on the vibrational modes of solids is similar to the results of neutron scattering and of inelastic X-ray spectroscopy, but it can be obtained from much smaller volumes. It is likely to become a standard characterization method for the vibrational and electronic properties of small crystals, highly competitive with established techniques. Another readily foreseeable application of vibrational spectroscopy was detecting energy gains, which had been observed with the Boersch/Geiger EELS instrument [44]. The experimentally determined gain/loss ratio was immediately put to a new use: measuring the local temperature of the sample with an accuracy of a few K [45,46]. The determination is completely standard-less and it can be done for nm-sized volumes of almost any material. It seems likely that it will become the preferred technique for monitoring the sample temperature in electron microscopy, e.g. while observing in-situ chemical reactions.

Vibrational spectroscopy is particularly sensitive to hydrogen, because strongly bonded hydrogen gives the highest-energy features in vibrational spectra, at 300–500 meV, with cross-sections comparable to the cross-section of the carbon K-edge [47,48]. With no radiation damage, single hydrogen atoms should therefore be detectable by vibrational mapping. In reality, however, radiation doses of a few tens of $e^-$/Å lead to significant hydrogen mass loss, and detecting a single hydrogen atom with atomic resolution by vibrational EELS is not very likely. Spreading the beam over a large area reduces the damage and using the aloof geometry nearly eliminates it. Both techniques have been successfully used for hydrogen detection [32,49,50], which is now seen as very straightforward with vibrational spectroscopy.

The aloof geometry has allowed hydrogen to be detected in water pockets created when a few layers of graphene, or BN comprising a few layers, are covered by water and then by a second layer of graphene or BN. Somewhat surprisingly, this sample geometry results in an indefinite retention of water in the microscope vacuum [51]. This work also showed that the substitution of deuterium for hydrogen results in a new peak corresponding to D-O vibration, demonstrating that vibrational spectroscopy allows electron microscopes to detect and

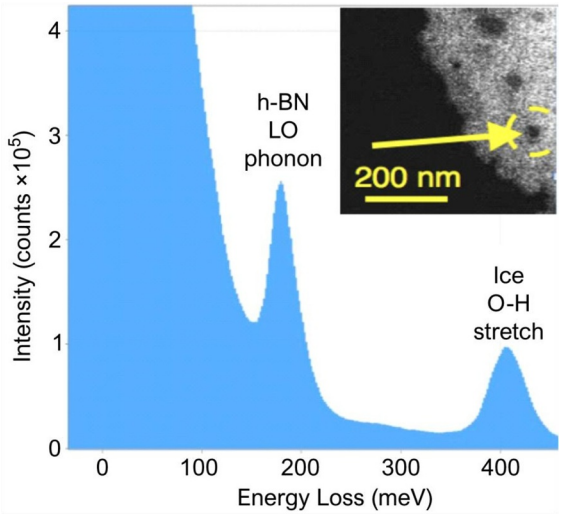


**Fig. 3.** Spectrum of ice held at about 100°K. The ice was grown on a BN flake, and both a BN phonon and a vibrational peak due to O—H stretch in ice are clearly resolved. 100 keV, 5 s acquisition time. The insert shows the sample; the spectrum was acquired with beam positioned in the center of the marked circle, and interacting with an area approximated by the dashed yellow circle.

potentially also to map isotopic substitution. It further demonstrated that hydrogen bonded to the carbon substrate films is a ubiquitous contaminant, probably tying up dangling bonds on and in the amorphous carbon. The fact that this contaminant does not seem to have been detected in electron microscopy before, even though carbon substrate films have been a staple of the technique since 80 years ago, is a testament to the new capabilities opened up by vibrational spectroscopy.

Another way to show the presence of hydrogen is to collect vibrational spectra of ice [52], as illustrated by Fig. 3. The ice was condensed onto a sample consisting of BN flakes resting on a holey carbon support, in the airlock of the Nion side entry stage. The water vapor was supplied by a silicone O-ring that was permeated with water by being boiled in it, and was placed near the sample as it was evacuated and cooled to liquid nitrogen temperature. Attempts to grow ice in the sample chamber of the Nion microscope were not successful–the vacuum around the sample was "dry", and no ice was detected even on samples that had been left cold in the microscope for an hour or more.

Spectra of the ice could be obtained using aloof geometry, but it turned out that the strongest spectra resulted when the probe was placed directly on the sample. It then rapidly drilled a hole in the ice, but continued to probe neighboring intact ice by "aloof" interaction with its surroundings. The hole radius was about 10 nm, and this meant that aloof interactions with the surrounding sample area could proceed very much as in the aloof geometry, but this time with the sample completely surrounding the electron beam.

A surprising and very welcome finding is that spectra obtained from holes drilled by the beam in ice and other materials including organic ones are very similar to aloof spectra collected with the beam outside the sample and not producing any visible damage. Valence spectra collected from a drilled hole, by comparison, do show important changes [49] and are not a good representation of the pristine material. Two effects probably make sure that drilling a hole in the sample does not affect vibrational spectra as strongly: (a) the vibrational features are excited from distances of several tens of nms and hence not as sensitive to the material immediately next to the hole, which has been damaged, and (b) vibrational spectra show distinct peaks due to different vibration modes, and different structural features give very distinct vibrational energies. Radiation damage next to the hole causes severe hydrogen loss, but the remaining hydrogen and other bonds are likely to give much the same vibrational spectra as before the damage.

A similar reduction in radiation damage is observed when the beam is scanned in a coarse raster pattern ("leapfrog" scan): rapid large advances of the probe with longer wait times at each pixel, which typically result in a regular array of holes drilled by the beam in radiation-sensitive samples [53]. Using this scanning pattern on guanine crystals with a spacing of 30 nm gave essentially no visible damage between the drilled holes and pristine vibrational spectra, whereas leapfrog spacing of 10 nm caused appreciable mass loss between the holes and significant reduction in intensity of the vibrational peaks [54].

The ice spectrum was obtained at 100 kV primary energy with about 20 meV energy resolution, for the simple reason that amorphous ice gives a broad hydrogen peak and better resolution was unlikely to produce more detailed spectra. Spectra from organic molecules such as guanine show that features due to different types of hydrogen bonds (to C vs. N) and stretch vs. scissors modes become resolvable at about 10 meV energy resolution [55]. However, to resolve finer features due to vibrations of the C—N rings, energy resolution of 5 meV or better is needed. This resolution was not available at the time of the guanine experiments, but it is available now. Fig. 4 compares log-linear plots of spectra of an L-alanine amino acid obtained with 15 meV and 5 meV energy resolution [56]. The higher resolution spectrum is vastly more informative, with a large number of peaks that can be used for fingerprinting, and the lowest identifiable features beginning at about 20 meV, whereas in the worse resolution spectrum there is a limited number of broad peaks and features even at 60 meV remain very weak. The improved visibility of low energy features is partly due to the faster cut-off of the ZLP tail, which is suppressed 5–10x more strongly at up to 400 meV in the higher resolution spectrum.

Fig. 5 shows a background-subtracted version of the higher resolution spectrum on a linear scale, together with a schematic representation of the L-alanine zwitterion molecule [57]. The spectrum encompasses the 50–250 meV loss region, which contains more than 10 characteristic peaks. Comparing this spectrum with one obtained from L-alanine in which the circled $^{12}C$ atom was substituted by $^{13}C$ showed that the peak at 200.5 meV, which is due to the C = O stretch vibration, shifts to 195.7 meV [57]. The shift magnitude was determined with 0.3 meV accuracy, and the spatial distribution of the two types of the molecule was mapped. These are major advances, and their importance is highlighted in the discussion section.

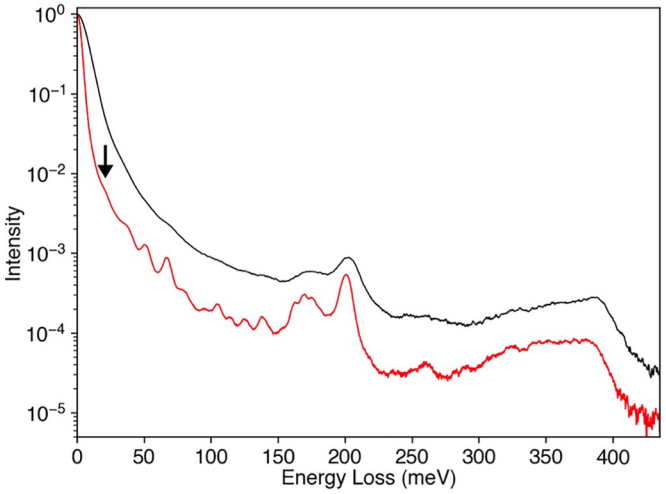


**Fig. 4.** Log-linear plots of vibrational spectra of L-alanine zwitterion acquired with 15 meV energy resolution at 60 keV (upper curve) and 5 meV resolution at 30 keV (lower curve). The spectra are normalized so that ZLP = 1, and the black arrow marks the beginning of recognizable features in the higher energy resolution spectrum.

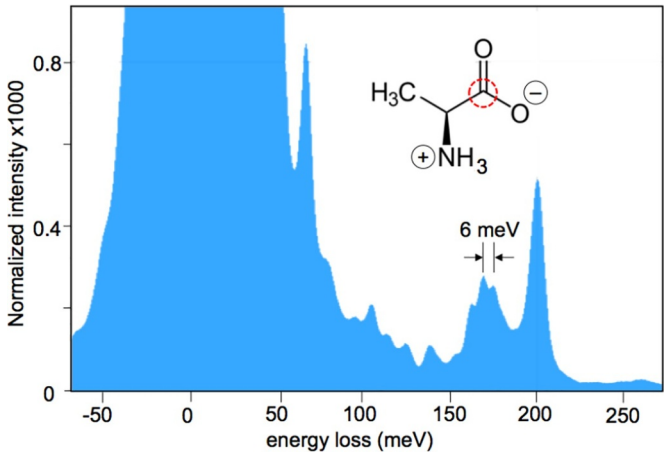


**Fig. 5.** Linear plot of spectrum of L-alanine zwitterion showing the 40–250 meV region in greater detail. Aloof acquisition with d ~ 20 nm at 30 keV. 100 separate spectra were acquired with acquisition time of 1.5 s each, aligned in energy, and added up, for a total acquisition time of 150 s. The intensity was scaled so that ZLP = 1. See Ref. [57] for similar spectra acquired from isotope-substituted L-alanine.

## 4. Future developments

The progress in energy resolution has come about because of our focus on enhanced stabilities, and on aberration correction. The focus on stability benefited from our experience in the design and construction of aberrations-corrected STEMs, in which an electron beam shaking by > 0.1 Å r.m.s. due to instabilities is readily noticeable [58,59]. Once the two most deleterious instabilities, due to HT and prism current variations, were rendered unimportant by our stabilization schemes, the key instability-reducing measures became much the same for EELS as for small probe formation in a STEM: decreasing the number and maximum strength of dipole-type deflectors, maximizing the stability of all power supplies, vibration-proof mechanical design, and thorough magnetic shielding. The result of these measures is that our system typically reaches ~1 meV r.m.s. short-term stability, and ~2 meV per minute energy drift (at 60 keV).

Aberration correction in the monochromator is needed for one simple reason: to maximize the monochromator transmissivity [60] so that a large beam current can be admitted into it while retaining good energy resolution. This consideration is very analogous to the need for aberration correction in STEM so that smaller probes with the same beam current can be formed, or same-size probes obtained with larger currents. It arises because the energy resolution $\delta E$ at the monochromator slit is limited by

$$\delta E \geq d_m/\kappa \tag{1}$$

where $d_m$ is the diameter of the electron beam at the slit for one unique electron energy (i.e., a perfectly monochromatic source), and $\kappa$ is the energy dispersion at the slit (typically measured in μm/eV). Improving the energy resolution therefore requires that beam diameter $d_m$ be reduced, or the energy dispersion $\kappa$ be increased, in the spectrum produced by the primary energy-dispersing element. (Magnifying the spectrum, as is done in our monochromator in order to make the demands on the mechanical quality of the energy-selecting slit less stringent, increases $d_m$ and $\kappa$ equally, and does not change the fundamental limit on the energy resolution.) Increasing the energy dispersion typically requires larger prisms, which are not practical and suffer ills such as greater cost, decreased mechanical rigidity and greater sensitivity to stray magnetic fields. This leaves decreasing the beam size $d_m$ as the more attractive option.

$d_m$ is determined by the factors familiar from STEM small probe formation:

$$d_m = (d_s^2 + d_d^2 + d_i^2)^{0.5} \tag{2}$$

where $d_s$ is the source size projected into the slit plane, $d_d$ the diffraction limit for the range of angles converging on the slit ($d_d = 0.61\ \lambda/\alpha$, where alpha is the half-angle of convergence at the slit), $d_i$ the probe broadening due to instabilities, and we assume that the beam angle incident on the slit is selected so that aberrations do not appreciably broaden the beam. $d_s$ depends on the current in the probe and the coherent current $I_c$ of the electron source as:

$$d_s = d_d(I_m/I_c)^{0.5} \tag{3}$$

where $I_m$ is the beam current incident on the monochromator slit.

When the instabilities are sufficiently minimized, the monochromator energy resolution is determined by $d_s$ and $d_d$, and opting for larger beam current coming into the monochromator $I_m$ results in worsened energy resolution. We typically set $I_m$ to 300–600 pA, i.e. about 2x–4x the CFEG's coherent current [58], and thus worsen the energy resolution potentially attainable by the monochromator by about 2x, while retaining enough current in the monochromated probe for imaging and analysis.

The path to better energy resolution in the monochromator is very clear: improving the quality of the aberration correction, which will allow the angular range in the main prism to be increased, the diffraction limit to be decreased, and the beam diameter $d_m$ at the slit to be made smaller (at the same beam current as before). We presently correct the aberrations at the slit to third order, and progressing to fifth order correction may become necessary in the future. A minor complication is that as the beam current admitted into the monochromator is made larger, the $C_s$ contribution from the gun becomes more important, and the 3rd order correction in the monochromator therefore needs to be retuned for each new setting of the coupling lenses between the gun and the monochromator. The complication becomes manageable by restricting the number of programmed settings of the coupling lenses.

The energy resolution in the spectrometer is governed by similar expressions, and aberration correction is even more important in the EELS than in the monochromator. This is because scattering at the sample increases both the angular range and the beam crossover size (i.e., the “phase space” occupied by the scattered beam), and thus a higher transmissivity is needed for the spectrometer than for the monochromator. We perform aberration correction up to 5th order, using multipole fields of all multiplicities up to rotatable 12-pole, produced by the pre-prism 16-pole assembly.

It is useful to note that the energy resolution of the whole monochromated microscope system is governed by many influences added in quadrature. This means that when the monochromator and the spectrometer are contributing equally to a final resolution of 4.2 meV, each one needs to attain an energy resolution of < 3 meV. Further developments are likely to improve the energy resolution in a similar way to how the spatial resolution of electron microscopes has been improving in the era of electron-optical aberration correction: more gradually after the initial major advances. A new potential problem may arise because the electron beam in the principal energy-dispersing prisms needs to be wide, so as to make the beam angles at the prism exits large and thereby minimize the diffraction-limited beam size $d_d$. The problem is instability due to magnetic Johnson noise [61,62], which affects wide beams more strongly and may require special mitigation measures.

The increased sophistication of the monochromator and the spectrometer does not mean that their everyday operation becomes an unapproachably complicated task. As with aberration correctors, the high-order aberrations are very stable and do not require daily tuning. Lower-order tuning is readily automated, for instance by tilting the beam before the sample while making sure it does not move on the sample in $x$ and $y$, and measuring the resultant energy shift in the EELS. User-friendly software carries out these adjustments automatically, much like the tuning of aberration correctors, which is typically

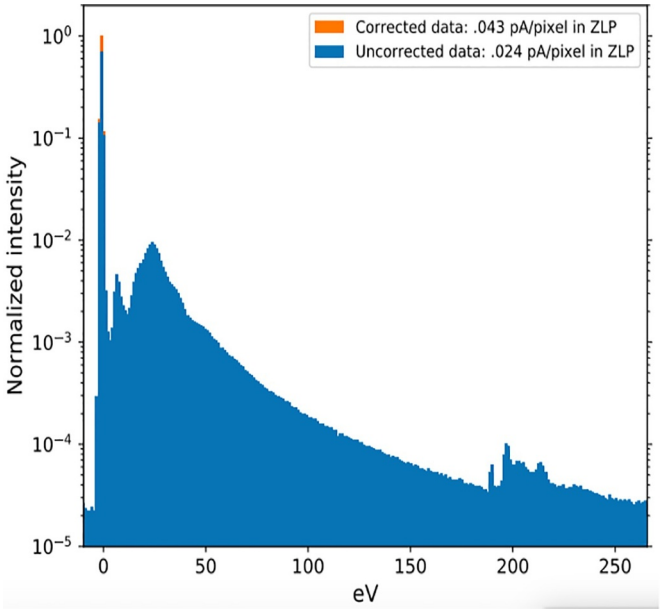


**Fig. 6.** Test of a Medipix3-based direct detector for EELS showing a spectrum of BN taken with 100 keV primary energy, 20,000 × 0.5 ms exposures (i.e., total exposure of 10 s), and DQE for single electrons ~0.8. The data are shown with (orange) and without (blue) correction for count rate non-linearity, which is only significant for the high intensity zero loss peak.

performed with equal ease by novice and expert operators alike.

Fundamental improvements can also be expected in the area of EELS detectors, which should ideally detect single electrons with detective quantum efficiency (DQE) close to 1, and further have a large dynamic range allowing ZLPs as intense as several hundred pA to be recorded without saturation, point spread function not much greater than 1 pixel, minimized ZLP tails, no afterglow or other temporary changes in detector locations where the ZLP was parked, and a large number of pixels, particularly in the energy dispersion direction.

Hybrid pixel detectors originally developed for X-ray detection but increasingly used in electron microscopy [63,64] satisfy several of these requirements. Fig. 6 shows a log-linear plot of an EEL spectrum of BN obtained with a Medipix3-type detector [65] prototype adapted for in-vacuum use. Although detectors with 1536 × 512 pixels and more are readily available, a single 256 × 256 chip was used for the present proof-of-principle test. The energy dispersion was set to about 1 eV per channel, and the spectrum includes both the zero loss peak and the boron K-edge at 188 eV energy loss. 20,000 spectra were recorded at 100 keV primary energy with 0.5 ms acquisition time and added together, for a total acquisition time of 10 s. The detector was able to record the spectrum with a point spread function only just wider than 1 pixel, as shown by the ZLP that drops to about 15% of the maximum intensity in adjacent pixels. Even more impressive is the spectrum to the left of the zero loss peak: the ZLP tail drops to $2 \times 10^{-5}$ of the ZLP maximum intensity just 3 pixels away from the ZLP center. It then stays at this level, making it likely that a re-scattering mechanism illuminating the whole chip was responsible.

The detector only operates in an electron-counting mode, which is a big plus for low spectrum intensities. The flip side is that each electron detection is followed by a 2 μsec dead time in that pixel of the Medipix3 detector, during which newly arriving electrons are not registered. This produces a count-rate saturation of about 0.03 pA per pixel, and a significant nonlinearity in the recorded count rate close to saturation. The nonlinearity can be compensated by characterizing the non-linear fall-off in the recorded intensity and correcting for it. This was done in the shown spectrum, in which the total current in the ZLP maximum was about 0.7 pA, and this intensity was spread in the non-dispersion direction over 16 pixels, giving 0.043 pA per pixel in the ZLP. Spreading the current across a whole detector in a 512 pixel wide detector array and allowing the ZLP to be 2 pixels wide in the dispersion direction would give a saturation current of about 30 pA, but this is on the low side for non-monochromated spectra which can have > 100 pA total beam current, especially when doing EELS elemental mapping. The EMPAD (electron microscope pixel array detector) developed at Cornell has a much higher saturation current of 3 pA per pixel [63], but it is not presently available in sizes larger than 128 × 128. However, large-format detectors in which the dead time is decreased to give similar saturation current as the EMPAD are under development, making it likely that a "nearly perfect" EELS detector will become available in the next few years.

## 5. Discussion

The ability to collect spectra rich in information on biological materials with highly reduced or no radiation damage, demonstrated by Figs 4 and 5, may turn out to be a very important development. Progress in phase-contrast cryo electron microscopy using low-dose techniques has allowed the structures of biological objects such as viruses and proteins to be solved at close to atomic resolution [66,67], provided that thousands or more identical copies of the objects are available. When combined with detailed knowledge of the chemical sequence making up the object, the structures typically lead to atomistic models of the virus or protein. However, when identical copies are not available or when the objects are embedded in biological tissue, phase contrast cryo-microscopy does not work nearly as well. It remains to be seen whether minimum-damage vibrational spectroscopy and mapping carried out on thin frozen biological sections at about 30 nm spatial resolution can bring complementary insights into structures such as proteins at cell membranes and other biological structures of great research interest.

In physics and materials science, < 5 meV vibrational spectroscopy is certain to bring many benefits. A recent example was provided by vibrational spectroscopy of $B_6P$ [68], a novel compound synthesized in small quantities at high pressures. 5 meV resolution vibrational spectra gave a comprehensive collection of peaks in the 40 meV–120 meV loss region, equally rich in detail as the L-alanine spectrum of Fig. 5. As the energy resolution and EELS detectors improve further, low-energy vibrational modes due to heavier elements will become increasingly accessible, and shed light on phonon modes and other properties of very small amounts of materials. Combined with variable-temperature sample stages, phenomena hitherto experimentally inaccessible are likely to yield many revealing insights.

## 6. Conclusion

In his seminal paper titled "A synchrotron in a microscope" presented at the 1997 EMAG meeting [69], Prof. Mick Brown, Archie Howie's longtime collaborator, showed how the STEM can acquire EELS data very similar to X-ray absorption spectra obtainable with synchrotrons, and wrote: "The STEM is already a high-performance synchrotron in a microscope." He then qualified the statement by adding "Of course, there are many things a STEM cannot do …, so it cannot supplant a new synchrotron".

Twenty one years later, the STEM also fulfills the roles of a sub-Å resolution imaging instrument with many contrast modes including highly flexible phase contrast, an efficient atomic-resolution elemental mapping machine, a single-atom detector and analyzer able to compete with SIMS and atom-probe, a neutron or inelastic X-ray scattering apparatus able to work with amounts of matter as small as $10^{-17}$ grams, and a high spatial resolution infrared spectrometer. Even though the STEM will of course not supplant these other instruments either, the combined effect of the various developments amounts to a revolution in electron microscopy. It is very gratifying that the developments have

followed paths pioneered by the three researchers honored in this issue: Christian Colliex, Archie Howie and Hannes Lichte.

## Acknowledgments

Partial support for developing the Nion Iris spectrometer was provided by DOE grant DE-SC0007694. J.A.H. and J.C.I. were supported by the Center for Nanophase Materials Sciences, which is a Department of Energy Office of Science User Facility, and the research was partly conducted using instrumentation within ORNL's Materials Characterization Core provided by UT-Battelle, LLC under Contract No. DE-AC05-00OR22725 with the U.S. Department of Energy. We are grateful to our colleagues at Nion Co., particularly to Petr Hrncirik, Dimitry Kudlay, Gwyn Skone and Zoltan Szilagyi for help with hardware, electronics and software, as well as bringing up and running the instruments. Special thanks are also due to Ray Carpenter, Phil Batson, Mathieu Kociak and Odile Stephan, whose help in launching the ultrahigh energy resolution EELS project at Nion has been invaluable, and to Mick Brown, Archie Howie, Peter Rez, Mike Walls and several others for enlightening discussions and encouragement.

## Conflict of interest

O.L. Krivanek, N. Dellby, M.T. Hotz, B. Plotkin-Swing, N.J. Bacon, A.L. Bleloch, G.J. Corbin, M.V. Hoffman, C.E. Meyer and T.C. Lovejoy are employees and/or officers of Nion Co., and have a financial interest in Nion.

## Supplementary materials

Supplementary material associated with this article can be found, in the online version, at doi:10.1016/j.ultramic.2018.12.006.

## References

[1] G. Galilei, Sidereus Nuncius, Apud Baglionum, Venice, 1610 See also https://www.universetoday.com/15763/galileos-telescope/.
[2] N. Lane, The unseen world: reflections on Leeuwenhoek (1677) 'concerning little animals, Phil. Trans. R. Soc. B370 (2015) 20140344.
[3] J. Hillier, On microanalysis by electrons, Phys. Rev. 64 (1943) 318–319.
[4] J. Hillier, R.F. Baker, Microanalysis by means of electrons, J. Appl. Phys. 15 (1944) 663–675.
[5] A.V. Crewe, M. Isaacson, D. Johnson, A high resolution electron spectrometer for use in transmission scanning electron microscopy, Rev. Sci. Instrum. 42 (1971) 411–420.
[6] M. Isaacson, M. Scheinfein, A high performance electron energy loss spectrometer for use with a dedicated STEM, J. Vac. Sci. Technol. B 1 (1983) 1338–1343.
[7] P.E. Batson, High resolution electron energy loss spectrometer for the scanning transmission electron microscope, Rev. Sci. Inst. 57 (1986) 43–48.
[8] A.V. Crewe, M. Isaacson, D. Johnson, Electron energy loss spectra of nucleic acid bases, Nature 231 (1971) 262–263.
[9] C. Colliex, V.E. Cosslett, R.D. Leapman, P. Trebbia, Contribution of electron energy loss spectroscopy to the development of analytical electron microscopy, Ultramicroscopy 1 (1976) 301–315.
[10] J.H. Paterson, O.L. Krivanek, ELNES of 3D transition metal oxides: II. Variation with oxidation state and crystal structure, Ultramicroscopy 32 (1990) 319–325.
[11] W. Wien, Die electrostatischen eigenschaften der kathodenstrahlen, Verhandl. Deut. Physik. Ges. 16 (1897) 165.
[12] H. Boersch, J. Geiger, W. Stickel, Das Auflösungsvermögen des elektrostatisch-magnetischen energieanalysators für schnelle elektronen, Zeitschrift für Phys. 180 (1964) 415–424.
[13] J. Geiger, Inelastic electron scattering with energy losses in the meV-region, in: G.W. Bailey (Ed.), Proceedings of the Thirty-ninth EMSA Meeting, Baton Rouge, LA, USA, Claitors, 1981, pp. 182–185.
[14] H. Ibach, Electron Energy Loss Spectrometers, Springer, Berlin and Heidelberg, 1991.
[15] K. Tsuno, Monochromators in electron microscopy, Nucl. Instrum. Methods Phys. Res. A645 (2011) 12–19.
[16] K. Kimoto, Practical aspects of monochromators developed for transmission electron microscopy, Microscopy 63 (2014) 337–344.
[17] P.W. Hawkes and O.L. Krivanek, Aberration correctors, monochromators, spectrometers, Springer Handbook of Microscopy, Springer, 2019.
[18] E. Essers, G. Benner, T. Mandler, S. Meyer, D. Mittmann, M. Schnell, R. Hoschen, Energy resolution of an omega-type monochromator and imaging properties of the MANDOLINE filter, Ultramicroscopy 110 (2010) 971–980.
[19] M. Terauchi, M. Tanaka, K. Tsuno, M. Ishida, Development of a high energy resolution electron energy-loss spectroscopy microscope, J. Microsc. 194 (1999) 203–209.
[20] H. Boersch, Experimentelle bestimmung der energieverteilung in thermisch ausgelösten elektronenstrahlen, Z. Phys. 139 (1954) 115.
[21] O.L. Krivanek, A.J. Gubbens, N. Dellby, Developments in EELS instrumentation for spectroscopy and imaging, Microsc. Microanal. Microstruct. 2 (1991) 315–332.
[22] O.L. Krivanek, J.P. Ursin, N.J. Bacon, G.J. Corbin, N. Dellby, P. Hrncirik, M.F. Murfitt, C.S. Own, Z.S. Szilagyi, High-energy-resolution monochromator for aberration-corrected scanning transmission electron microscopy/electron energy-loss spectroscopy, Phil. Trans. R. Soc. A367 (2009) 3683–3697.
[23] O.L. Krivanek and N. Dellby, US Patent #8,373,137 B2 (2013).
[24] O.L. Krivanek, T.C. Lovejoy, N. Dellby, R.W. Carpenter, Monochromated STEM with a 30 meV-wide, atom-sized electron probe, Microscopy 62 (2013) 3–21.
[25] A.J. Gubbens, M. Barfels, C. Trevor, R. Twesten, P.E. Mooney, P. Thomas, N. Menon, B. Kraus, C. Mao, B. McGinn, The GIF quantum, a next generation post-column imaging energy filter, Ultramicroscopy 110 (2010) 962–970.
[26] O.L. Krivanek, T.C Lovejoy, M.F. Murfitt, G. Skone, P.E. Batson, N. Dellby, Towards sub-10 meV energy resolution STEM-EELS, J. Phys. Conf. Ser. 522 (2014) 012023.
[27] H. Cohen, P. Rez, T. Aoki, P.A. Crozier, N. Dellby, Z. Dellby, D. Gur, T.C. Lovejoy, K. March, M.C. Sarahan, S.G. Wolf and O.L. Krivanek, Hydrogen Analysis by Ultra-High Energy Resolution EELS, Microsc. Microanal. 21 (Suppl 3), (2015) 661–662.
[28] T.C. Lovejoy, G.C. Corbin, N. Dellby, M.V. Hoffman, O.L. Krivanek, Advances in ultra-high energy resolution STEM-EELS, Microsc. Microanal. 24 (Suppl 1) (2018) 446–447.
[29] O.L. Krivanek, A.L. Bleloch, N. Dellby, T.C. Lovejoy, C. Shi, W. Zhou, Improving the STEM spatial resolution limit, Microsc. Microanal. 24 (Suppl 1) (2018) 18–19.
[30] Q. Liu, L. Zhang, K. March, T. Aoki, P.A. Crozier, Bandgaps and surface inter-band states in photocatalysts with high energy resolution EELS, Microsc. Microanal. 21 (Suppl 3) (2015) 1903–1904.
[31] D.M. Haiber, T. Aoki, P.A. Crozier, Exploring vibrational and electronic structure of carbon nitride powders using monochromated electron energy-loss spectroscopy, Microsc. Microanal. 22 (Suppl 3) (2016) 986–987.
[32] O.L. Krivanek, T.C. Lovejoy, N. Dellby, T. Aoki, R.W. Carpenter, P. Rez, E. Soignard, J. Zhu, P.E. Batson, M.J. Lagos, R.F. Egerton, P.A. Crozier, Vibrational spectroscopy in the electron microscope, Nature 514 (2014) 209–212.
[33] T. Miyata, M. Fukuyama, A. Hibara, E. Okunishi, M. Mukai, T. Mizoguchi, Measurement of vibrational spectrum of liquid using monochromated scanning transmission electron microscopy–electron energy loss spectroscopy, Microscopy 63 (2014) 377–382.
[34] P.E. Batson, Surface plasmon coupling in clusters of small spheres, Phys. Rev. Lett. 49 (1982) 936–940.
[35] P.E. Batson, A new surface plasmon resonance in clusters of small spheres, Ultramicroscopy 9 (1982) 277–282.
[36] M.G. Walls, A. Howie, Dielectric theory of localised valence energy loss spectroscopy, Ultramicroscopy 28 (1989) 40–42.
[37] F.J. Garcia de Abajo, A. Howie, Electron spectroscopy from the outside–aloof beam or near field? Inst. Phys. Conf. Ser. 161 (1999) 327–330.
[38] H. Cohen, T. Maniv, R. Tenne, Y. Rosenfeld, H. Cohen, O. Stephan, C. Colliex, Near-field electron energy loss spectroscopy of nanoparticles, Phys. Rev. Lett. 80 (1998) 782–785.
[39] C. Dwyer, T. Aoki, P. Rez, S.L.Y. Chang, T.C. Lovejoy, O.L. Krivanek, Electron-beam mapping of vibrational modes with nanometer spatial resolution, Phys. Rev. Lett. 117 (2016) 256101.
[40] M.J. Lagos, A. Trügler, U. Hohenester, P.E. Batson, Mapping vibrational surface and bulk modes in a single nanocube, Nature 453 (2017) 529–532.
[41] U. Hohenester, A. Trügler, P.E. Batson, M.J. Lagos, Inelastic vibrational bulk and surface losses of swift electrons in ionic nanostructures, Phys. Rev. B 97 (2018) 165418.
[42] A.A. Govyadinov, A. Konečná, A. Chuvilin, S. Vélez, I. Dolado, A.Y. Nikitin, S. Lopatin, F. Casanova, L.E. Hueso, J. Aizpurua, R. Hillenbrand, Probing low-energy hyperbolic polaritons in van der Waals crystals with an electron microscope, Nature Commun. 8 (2017) 95, , https://doi.org/10.1038/s41467-017-00056-y.
[43] F.S. Hage, R.J. Nicholls, J.R. Yates, D.G. McCulloch, T.C. Lovejoy, N. Dellby, O.L. Krivanek, K. Refson and Q.M. Ramasse, Nanoscale momentum-resolved vibrational spectroscopy, Sci. Adv. 4 (2018) eaar7495.
[44] H. Boersch, J. Geiger, W. Stickel, Interaction of 25-keV electrons with lattice vibrations in LiF. Experimatal evidence of surface modes of lattice vibration, Phys. Rev. Lett. 17 (1966) 379–381.
[45] J.-C. Idrobo, A.R. Lupini, T. Feng, R.R. Unocic, F.S. Walden, DS. Gardiner, T.C. Lovejoy, N. Dellby, S.T. Pantelides, O.L. Krivanek, Temperature measurement by a nanoscale electron probe using energy gain and loss spectroscopy, Phys. Rev. Lett. 120 (2018) 095901.
[46] M.J. Lagos, P.E. Batson, Thermometry with subnanometer resolution in the electron microscope using the principle of detailed balancing, Nano Lett. 18 (2018) 4556–4563.
[47] P. Rez, Is localized infrared spectroscopy now possible in the electron microscope? Microsc. Microanal. 20 (2014) 671–677.
[48] C. Dwyer, Localization of high-energy electron scattering from atomic vibrations, Phys. Rev. B 89 (2014) 054103.
[49] P.A. Crozier, T. Aoki, Q. Liu, Detection of water and its derivatives on individual nanoparticles using vibrational electron energy-loss spectroscopy, Ultramicroscopy 169 (2016) 30–36.
[50] D.M. Haiber, P.A. Crozier, Nanoscale probing of local hydrogen heterogeneity in disordered carbon nitrides with vibrational electron energy-loss spectroscopy, ACS Nano 12 (2018) 5463–5472.

[51] J.R. Jokisaari, J. Hachtel, X. Hu, A. Mukherjee, C. Wang, A. Konečná, T.C. Lovejoy, N. Dellby, J. Aizpurua, O.L. Krivanek, J.-C. Idrobo, R.F. Klie, Vibrational spectroscopy of water with high spatial resolution, Adv. Mater. 30 (2018) 1802702.
[52] M.T. Hotz, G.C. Corbin, N. Dellby, T.C. Lovejoy, G. Skone, J.-D. Blazit, M. Kociak, O. Stephan, M. Tencé, H.W. Zandbergen, O.L. Krivanek, Optimizing the Nion STEM for In-Situ Experiments, Microsc. Microanal. 24 (Supplement S1) (2018) 1132–1133.
[53] R.F. Egerton, T. Aoki, P.A. Crozier, Taking advantage of scattering delocalization to reduce radiation damage in vibrational or valence-loss EELS and energy-filtered tem images, Microsc. Microanal. 22 (Suppl 3) (2016) 960–961.
[54] P. Rez, Private communication (2016).
[55] P. Rez, T. Aoki, K. March, D. Gur, O.L. Krivanek, N. Dellby, T.C. Lovejoy, S.G. Wolf, H. Cohen, Damage-free vibrational spectroscopy of biological materials in the electron microscope, Nature Commun. 7 (2016) 10945, https://doi.org/10.1038/ncomms10945.
[56] J.A. Hachtel and J.-C. Idrobo, Private communication (2018).
[57] J.A. Hachtel, J. Huang, I. Popovs, S. Jansone-Popova, J.K. Keum, J. Jakowski, T.C. Lovejoy, N. Dellby, O.L. Krivanek, J.-C. Idrobo, Identification of site-specific isotopic labeling in amino acids by vibrational spectroscopy in the electron microscope, Science (2018) In press.
[58] O.L. Krivanek, M.F. Chisholm, N. Dellby, M.F. Murfitt, Atomic-resolution STEM at low primary energies, in: S.J. Pennycook, P.D. Nellist (Eds.), Scanning Transmission Electron Microscopy: Imaging and Analysis, Springer, Berlin-Heidelberg-New \sYork, 2011, pp. 613–656.
[59] N. Dellby, N.J. Bacon, P. Hrncirik, M.F. Murfitt, G.S. Skone, Z.S. Szilagyi, O.L. Krivanek, Dedicated STEM for 200 to 40keV operation, Eur. Phys. J. Appl. Phys. 54 (2011) 33505.
[60] O.L. Krivanek, S.L. Friedman, A.J. Gubbens, B. Kraus, An imaging filter for biological applications, Ultramicroscopy 59 (1995) 267–282.
[61] S. Uhlemann, H. Müller, P. Hartel, J. Zach, M. Haider, Thermal magnetic field noise limits resolution in transmission electron microscopy, Phys. Rev. Lett. 111 (2013) 046101.
[62] A. Howie, Continued skirmishing on the wave-particle frontier, This volume (2019).
[63] M.W. Tate, P. Purohit, D. Chamberlain, K.X. Nguyen, R. Hovden, C.S. Chang, P. Deb, E. Turgut, J.T. Heron, D.G. Schlom, D.C. Ralph, G.D. Fuchs, K.S. Shanks, H.T. Philipp, D.A. Muller, S.M. Gruner, High dynamic range pixel array detector for scanning transmission electron microscopy, Microsc. Microanal. 22 (2016) 237–249.
[64] J.A. Mir, R. Clough, R. MacInnes, C. Gough, R. Plackett, I. Shipsey, H. Sawada, I. MacLaren, R. Ballabriga, D. Maneuski, V. O'Shea, D. McGrouther, A.I. Kirkland, Characterisation of the Medipix3 detector for 60 and 80keV electrons, Ultramicroscopy 182 (2017) 44–53.
[65] http://www.x-spectrum.de/index_htm_files/X-Spectrum_datasheet_250K.pdf.
[66] E. Callaway, The revolution will not be crystallized, Nature 525 (2015) 172–175.
[67] S. Subramaniam, W. Kühlbrandt, R. Henderson, CryoEM at IUCrJ: a new era, IUCrJ 3 (2016) 3–7.
[68] D. Taverna et al., In press (2018).
[69] L.M. Brown, A synchrotron in a microscope, in: J.M. Rodenburg (Ed.), Electron Microscopy and Analysis 1997, Institute of Physics Conference Series, 153 IOP Publishing, London, 1997, pp. 17–22.